INORGANIC CHEMISTRY FRONTIERS

RESEARCH ARTICLE

View Article Online
View Journal | View Issue

Cite this: *Inorg. Chem. Front.*, 2022, **9**, 959

Ferrocene-sensitized titanium-oxo clusters with effective visible light absorption and excellent photoelectrochemical activity†

Chao Wang, * Shoujuan Wang, Fangong Kong and Ning Chen

Sensitized Ti-oxo clusters have attracted growing attention as analogous molecular model compounds of dye-sensitized titanium dioxide solar cells. However, reports on the introduction of metal complexes as photosensitizers into Ti-oxo clusters are still very rare. Herein, with the use of an organometallic complex ferrocene as a sensitizer, two novel ferrocene-sensitized Ti-oxo clusters, namely, $[Ti_8(\mu_3\text{-}O)_4(Dipa)_2(Fcdc)_4(O^iPr)_{10}]\cdot 2HO^iPr$ (H_2Fcdc = 1,1-ferrocene dicarboxylic acid, Dipa = diisopropanolamine, and HO^iPr = isopropanol, **Ti_8Fcdc_4**) and $[Ti_{10}(\mu_4\text{-}O)_2(\mu_3\text{-}O)_4(Fcdc)_2(\mu_2\text{-}OEt)_8(OEt)_{10}]\cdot 2HOEt$ (**$Ti_{10}Fcdc_2$**) have been successfully synthesized. Their molecular structures, light absorption, charge transfer, and photoelectrochemical properties were systematically investigated. It is demonstrated that the incorporation of Fcdc ligands shows a significant influence on the light absorption of the resulting clusters, and their absorption band edge is extended to about 580 nm. Furthermore, experimental measurements and theoretical calculations showed that the intense intramolecular charge transfer occurs from the Fcdc ligands to the Ti-oxo core. Based on these advantages, clusters **Ti_8Fcdc_4** and **$Ti_{10}Fcdc_2$** were used as photoelectrode precursors to carry out photoelectrochemical experiments, and both exhibited clear photocurrent responses. The molecular structure, light absorption, and effective charge transfer of materials have a direct bearing on their photoelectrochemical performances. This work not only provides novel structural models for sensitized Ti-oxo clusters towards the modulation of photoelectric properties but also provides new insights into further understanding the structure–property relationships of sensitized clusters.

Received 11th November 2021,
Accepted 11th January 2022

DOI: 10.1039/d1qi01410b

rsc.li/frontiers-inorganic

Introduction

Developing new semiconductor materials to utilize solar energy is a promising method to solve environmental pollution and energy shortage.[1–3] Titanium dioxide materials have always been regarded as one of the most popular semiconductor materials due to their good stability and high photoactivity.[4–11] Nowadays, crystalline titanium-oxo cluster materials, as good molecular model compounds of titanium dioxide semiconductors, have attracted growing interest.[12–18] The potential motivation not only comes from the intrinsic properties of the titanium dioxide materials but also lies in the acquisition of precise molecular structural information, which contributes to further theoretical calculation and mechanistic explanations.[19–39] However, the light absorption of traditional Ti-oxo clusters is usually limited to the ultraviolet region, which greatly hinders the highly efficient utilization of solar energy. Ligand modification has been proven to be one of the effective solutions to reduce the band gap of traditional Ti-oxo clusters.[40–45] It is demonstrated that the electronic effect of ligands can effectively regulate the light absorption of the Ti-oxo clusters owing to the intense electronic interactions between the ligands and the Ti-oxo core.[46–51] Consequently, reasonable optimization of functionalized ligands is very important for the synthesis of novel titanium-oxo clusters with a narrow band gap and excellent photophysical and photochemical properties.

Organometallic complex ferrocene, as an efficient and stable electron donor, has been widely used in the construction of a variety of molecular materials.[52] Many ferrocene-functionalized complexes have been reported to date.[53] However, to the best of our knowledge, there are only a few examples of Ti-oxo clusters with ferrocene-derived functional ligands being reported.[54–61] Dai and Fan's groups made a great contribution in this field and synthesized a series of ferrocene-sensitized Ti-

State Key Laboratory of Biobased Material and Green Papermaking, Qilu University of Technology (Shandong Academy of Sciences), Jinan, 250353, China.
E-mail: wangchao@qlu.edu.cn

†Electronic supplementary information (ESI) available. CCDC 2119700 (**Ti_8Fcdc_4**) and 2119701 (**$Ti_{10}Fcdc_2$**). For ESI and crystallographic data in CIF or other electronic format see DOI: 10.1039/d1qi01410b

oxo clusters.[55–59] More recently, Lan and co-workers reported the synthesis and CO_2 photoreduction of ferrocene-sensitized Ti-oxo clusters.[60] It is worth mentioning that Liu's group synthesized the biggest ferrocene-sensitized $\{Ti_{22}Fc_4\}$ cluster.[61] Despite the above successful cases, the diversity of ferrocene-sensitized Ti-oxo clusters applied in structural model research studies is still unknown. In addition, the structure–property relationship of ferrocene-sensitized Ti-oxo clusters is worth further investigation.

We have been working on the synthesis, structure, and photorelated properties of Ti-oxo clusters.[62–67] In continuation of our research and in consideration of the characteristics of the ferrocene ligands, we carried out research on the synthesis of ferrocene-sensitized Ti-oxo clusters and their photoelectrochemical properties. Herein, two novel ferrocene-sensitized Ti-oxo clusters, namely, $[Ti_8(\mu_3\text{-}O)_4(Dipa)_2(Fcdc)_4(O^iPr)_{10}]\cdot 2HO^iPr$ (Dipa = diisopropanolamine and HO^iPr = isopropanol, **Ti_8Fcdc_4**) and $[Ti_{10}(\mu_4\text{-}O)_2(\mu_3\text{-}O)_4(Fcdc)_2(\mu_2\text{-}OEt)_8(OEt)_{10}]\cdot 2HOEt$ (HOEt = ethanol, **$Ti_{10}Fcdc_2$**), are successfully synthesized and structurally characterized. The light absorption, charge transfer, and photoelectrochemical properties of these two Ti-oxo clusters are investigated. We found that the light absorption range of clusters **Ti_8Fcdc_4** and **$Ti_{10}Fcdc_2$** can be significantly extended to the visible-light region, which is mainly caused by the intense intramolecular charge transfer from the Fcdc electron donor to the Ti-oxo core. Furthermore, the light absorption and the molecular structures of the resulting clusters have a direct bearing on their photoelectrochemical activity. Notably, the bridged Fcdc ligands in cluster **Ti_8Fcdc_4** can provide additional transmission channels for charge transfer between the two sub-clusters, thereby achieving enhanced photocurrent response (higher photoinduced charge transfer rate) in comparison with that of cluster **$Ti_{10}Fcdc_2$**. Our work provides novel structural models for sensitized Ti-oxo clusters towards understanding the electron communication mechanism and regulating the photoelectric properties.

Experimental

Reagents and instrumentation

$Ti(O^iPr)_4$ (97%), 1,1-ferrocene dicarboxylic acid (98%), diisopropanolamine (98%), isopropanol (99.5%), and ethanol were purchased from Aladdin. X-ray diffraction (XRD) data were collected using a Bruker D_8 Focus diffractometer (CuKα, λ = 1.5406 Å). Thermogravimetric analysis (TGA) data of the cluster samples were recorded using a TGAQ50 instrument. UV–vis spectra were obtained using a Cary 4000 UV–vis spectrophotometer. Infrared spectroscopy (IR) measurements were performed using a Nicolet 6700 spectrometer. X-ray photoelectron spectroscopy (XPS) investigation was performed using a Thermo Scientific ESCALABXi + instrument.

Crystal structure determination

An Agilent Gemini E diffractometer with an Eos CCD detector was used to collect the crystallographic data of the clusters. The structures are solved by the inherent phase method in the SHELXT program and refined by the least square method in the SHELXL program.[68] Both programs are used coupling with OLEX2.[69] Some restraints such as DFIX, SADI, DELU, and SIMU were applied. Table S1† shows unit-cell and refinement parameters. CCDC 2119700 and 2119701 (**Ti_8Fcdc_4** and **$Ti_{10}Fcdc_2$**) contain additional crystallographic details.†

Photoelectrochemistry (PEC) measurements

All photoelectrochemistry measurements (photocurrent, the Mott–Schottky plots and electrochemical impedance spectra) were carried out using a CHI660E electrochemical workstation in a three-electrode system, with the sample coated indium tin oxide (ITO) glass as the working electrode, a Pt wire as the counter electrode, and a saturated Ag/AgCl electrode as the reference electrode. The working electrode was ITO glass plates coated with a cluster-slurry and the electrolyte was Na_2SO_4 (0.2 M) aqueous solution. For the preparation of working photoelectrodes, the crystal sample (about 3 mg) was dissolved in ethanol (1 mL), which was then dropped onto a precleared ITO glass (1 cm^2). The working photoelectrode was obtained after evaporation. The Mott–Schottky plots were also measured over an alternating current frequency of 1000 Hz. Electrochemical impedance spectra (EIS) measurements were recorded over a frequency range of 100 kHz–0.1 Hz.

Synthesis of Ti_8Fcdc_4

H_2Fcdc (27.4 mg, 0.1 mmol), diisopropanolamine (66.60 mg, 0.50 mmol) and isopropanol (5 mL) were added into a Teflon-lined autoclave with stirring for 10 min, and then combined with $Ti(O^iPr)_4$ (100 μL, 0.3 mmol). The resultant mixture was transferred to a pre-heated oven at 100 °C for 3 days. Yellow crystals were obtained after cooling down. Yield: *ca.* 65% (based on $Ti(O^iPr)_4$). Infrared spectroscopy data (cm^{-1}): 2970 (w), 2933 (w), 2884 (w), 1581 (m), 1495 (s), 1416 (s), 1379 (s), 1213 (w), 1144 (s), 997 (s), 947 (m), 863 (w), 785 (s), 721 (w), 611 (m), 524 (m).

Synthesis of $Ti_{10}Fcdc_2$

H_2Fcdc (27.4 mg, 0.1 mmol) and ethanol (5 mL) were added into a Teflon-lined autoclave with stirring for 10 min, and then combined with $Ti(O^iPr)_4$ (100 μL, 0.3 mmol). The resultant mixture was then transferred to a pre-heated oven at 100 °C for 3 days. Yellow crystals were obtained after cooling down. Yield: *ca.* 70% (based on $Ti(O^iPr)_4$). Infrared spectroscopy data (cm^{-1}): 2970 (w), 2923 (w), 2884 (w), 1576 (m), 1475 (s), 1383 (s), 1337 (s), 1148 (s), 1097 (s), 996 (s), 946 (m), 905 (w), 877 (w), 716 (w), 619 (m), 527 (m).

Results and discussion

Synthesis

Herein solvothermal synthesis was adopted to isolate ferrocene-sensitized Ti-oxo clusters. With the use of H_2Fcdc as a ligand, two novel ferrocene-sensitized Ti-oxo clusters were suc-

cessfully synthesized with relatively high yields. In the course of the synthesis of **Ti_8Fcdc_4** and **$Ti_{10}Fcdc_2$**, we found that the solvent plays a crucial role in their crystallization process. With the use of isopropanol as a solvent, yellow crystals of **Ti_8Fcdc_4** were successfully obtained in the presence of Dipa. When isopropanol was replaced by ethanol, yellow crystals of **$Ti_{10}Fcdc_2$** were successfully obtained. The crystal pictures and the assembly unit of clusters **Ti_8Fcdc_4** and **$Ti_{10}Fcdc_2$** are shown in Fig. 1a and f, respectively. Structurally, **Ti_8Fcdc_4** is an octanuclear cluster consisting of two Ti_4 motifs connected by two Fcdc ligands (Fig. S1†); and **$Ti_{10}Fcdc_2$** is a ten-nuclear cluster that is constructed from two Ti_5 units bridged by two μ_3-O atoms (Fig. S1†). The detailed structural description can be found in the structural discussion section.

Crystal structure of Ti_8Fcdc_4

The structure of cluster **Ti_8Fcdc_4** crystallizes in the space group $P2_1/n$. As shown in Fig. 1b, four Ti atoms, two Fcdc ligands, two μ_3-O atoms, six $-O^iPr$ groups, and a free HO^iPr molecule compose the asymmetric unit of cluster **Ti_8Fcdc_4**. In the structure of cluster **Ti_8Fcdc_4**, four Ti atoms are connected by two μ_3-O atoms to form the $Ti_4(\mu_3\text{-}O)_2$ unit, which is further linked with one Fcdc ligand and one Dipa molecule. The two $Ti_4(\mu_3\text{-}O)_2$ units are connected by two Fcdc units to construct the structure of octa-nuclear cluster **Ti_8Fcdc_4** (Fig. 1c). The two oxygen atoms of the carboxylic acid in the Fcdc unit (Fe1) are coordinated with Ti3 and Ti4 in the same $Ti_4(\mu_3\text{-}O)_2$ unit and Ti2 and Ti4 in another $Ti_4(\mu_3\text{-}O)_2$ unit, at the same time, the four oxygen atoms of the carboxylic acids in the Fcdc units (Fe2) are coordinated with four Ti atoms in a $Ti_4(\mu_3\text{-}O)_2$ unit (Fig. 1d). Furthermore, Ti1, Ti2, and Ti3 in the $Ti_4(\mu_3\text{-}O)_2$ unit are also connected to two oxygen and one nitrogen of diisopropanolamine, and the Ti–O core of cluster **Ti_8Fcdc_4** is connected with twelve terminal $-O^iPr$ groups. Different from the reported $\{Ti_{22}Fc\}$ structure,[61] the Fcdc ligand in **Ti_8Fcdc_4** exhibits two coordination modes, and this phenomenon is rare in Ti-based coordination compounds. Similar to that of reported ferrocene-sensitized Ti-oxo clusters,[56–60] Ti atoms (Ti2, Ti3, and Ti4) in the $Ti_4(\mu_3\text{-}O)_2$ unit are also six-coordinate with a slightly distorted octahedral geometry configuration, while the Ti1 atom is seven-coordinate with a pentagonal bipyramid coordination environment (Fig. 1e). Furthermore, the clusters are stacked into a three-dimensional supramolecular structure. However, there are no obvious interactions between the adjacent clusters (Fig. S3†).

Crystal structure of $Ti_{10}Fcdc_2$

The structure of cluster **$Ti_{10}Fcdc_2$** crystallizes in the space group $P\bar{1}$. Structurally, the asymmetric unit of cluster **$Ti_{10}Fcdc_2$** involves five Ti atoms, one Fcdc ligand, one μ_4-O atom, two μ_3-O atoms, twelve –OEt groups, and one HOEt molecule (Fig. 1g). In cluster **$Ti_{10}Fcdc_2$**, titanium atoms (Ti1, Ti2, Ti3, and Ti4) are connected with one μ_4-oxygen atom to form a $Ti_4(\mu_4\text{-}O)$ unit, and it is further connected to Ti5 by two μ_3-oxygen atoms to form a $Ti_5(\mu_4\text{-}O)(\mu_3\text{-}O)_2$ unit (Fig. 1h). At the same time, two $Ti_5(\mu_4\text{-}O)(\mu_3\text{-}O)_2$ units are bridged *via* two μ_3-O atoms to construct the structure of a ten-nuclear cluster **$Ti_{10}Fcdc_2$** (Fig. 1i). The four oxygen atoms of the Fcdc ligands are coordinated with the four Ti atoms (Ti1, Ti2, Ti3 and Ti5), respectively. Different from the peripheral $-O^iPr$ groups of the

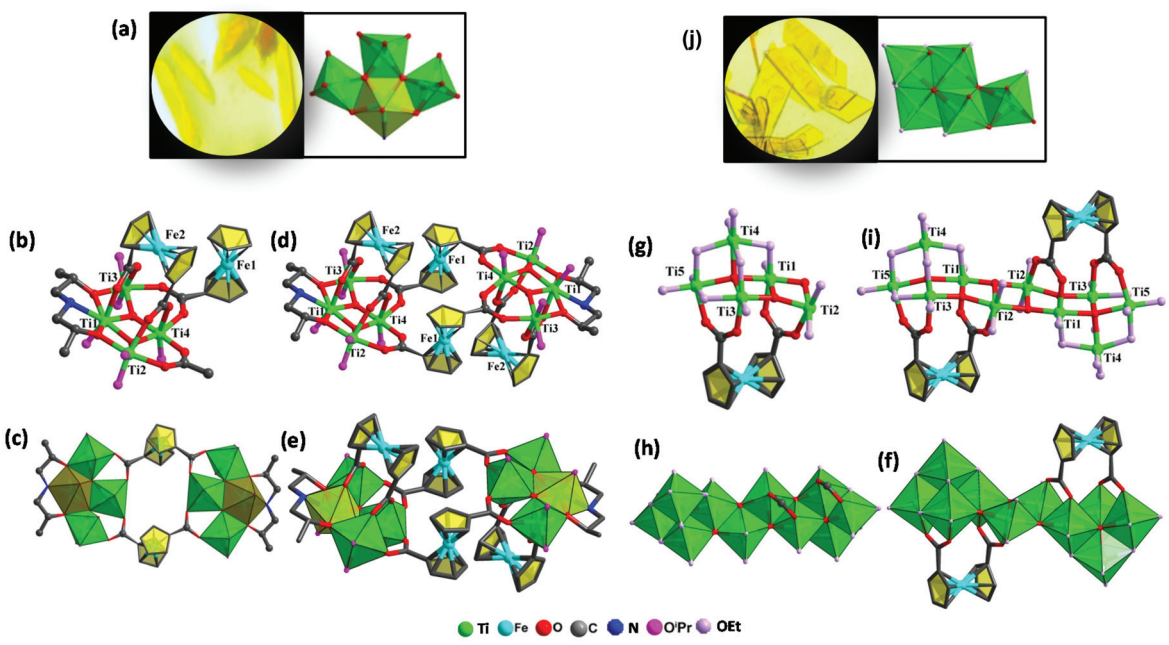

Fig. 1 (a) The crystal picture and the Ti_4 unit of **Ti_8Fcdc_4**. (b) The asymmetric unit of **Ti_8Fcdc_4**. (c) The Ti-oxo core of **Ti_8Fcdc_4**. (d) The ball-stick structure of **Ti_8Fcdc_4**. (e) The polyhedral structure of **Ti_8Fcdc_4**. (f) The crystal picture and the Ti_5 unit of **$Ti_{10}Fcdc_2$**. (g) The asymmetric unit of **$Ti_{10}Fcdc_2$**. (h) The Ti-oxo core of **$Ti_{10}Fcdc_2$**. (i) The ball-stick structure of **$Ti_{10}Fcdc_2$**. (j) The polyhedral structure of **$Ti_{10}Fcdc_2$**.

Ti_8Fcdc_4 cluster core, the Ti–O core of the $Ti_{10}Fcdc_2$ cluster is coordinated with 22 –OEt groups (Fig. 1f). Similar to that of the reported ferrocene-sensitized Ti-oxo clusters,[57–61] the ten Ti atoms in cluster $Ti_{10}Fcdc_2$ are also six-coordinated with a slightly distorted octahedral geometry (Fig. 1g). Furthermore, the clusters are stacked into a three-dimensional supramolecular structure. However, there are no obvious interactions between the adjacent clusters (Fig. S4†).

The PXRD patterns of clusters Ti_8Fcdc_4 and $Ti_{10}Fcdc_2$ are highly consistent with the simulation results based on accurate crystallographic data (Fig. S5 and S6†), indicating their high purity. The TGA curves show that clusters Ti_8Fcdc_4 and $Ti_{10}Fcdc_2$ have favourable thermal stability with the onset temperature of thermal decomposition above about 250 °C, and 270 °C, respectively (Fig. S7 and S8†). Fig. S9 and S10† show the IR spectra of clusters Ti_8Fcdc_4 and $Ti_{10}Fcdc_2$. The bands of about 1000 cm^{-1} are designated as the Ti–O–C vibrations and the bands of about 610 cm^{-1} are designated as the Ti–O vibration. The bands between 2970 and 2884 cm^{-1} are designated as the C–H vibrations. Notably, the bands of about 1475 or 1490 cm^{-1} belong to the characteristic bands of the Fcdc moieties.

The valence states of Ti and Fe atoms within clusters Ti_8Fcdc_4 and $Ti_{10}Fcdc_2$ are identified by X-ray photoelectron spectroscopy (XPS). As shown in Fig. 2, the Ti 2p spectra clearly show that two peaks at 458.8 eV and 464.6 eV refer to the states of Ti $2p_{2/3}$ and Ti $2p_{1/2}$, respectively, indicating that only Ti^{4+} exists in clusters Ti_8Fcdc_4 and $Ti_{10}Fcdc_2$. The Fe 2p spectra clearly display that two peaks at 708.1 eV and 720.8 eV, respectively, refer to the states of Fe $2p_{2/3}$ and Fe $2p_{1/2}$, indicating the unique existence of Fe^{2+} in clusters Ti_8Fcdc_4 and $Ti_{10}Fcdc_2$.

Fig. 3a shows the solid-state UV–vis spectra of clusters Ti_8Fcdc_4 and $Ti_{10}Fcdc_2$. It can be clearly seen that clusters Ti_8Fcdc_4 and $Ti_{10}Fcdc_2$ exhibit broad absorption bands, and the absorption band edges are extended to about 580 and 560 nm, respectively, which is consistent with their yellow colour crystals. As generally accepted, the UV-light absorption band is mainly attributed to the O → Ti charge transfer in the Ti-oxo core. The extended visible absorption band is mainly induced by the charge transfer from the Fcdc ligands to the Ti-oxo core, as that for the reported Ti-oxo clusters functionalized by ferrocene ligands.[56–61] According to the Kubelka–Munk function $F(R) = (1 - R)^2/2R$, the estimated band gap energy of clusters Ti_8Fcdc_4 and $Ti_{10}Fcdc_2$ is about 2.05 and 2.10 eV, respectively (Fig. 3b). In the ferrocene-sensitized Ti-oxo cluster system, the charge of the ferrocene groups is delocalized to the Ti-oxo core owing to the π conjugation (between the carboxylic acid bond and cyclopentadiene ring) in the ferrocene ligand, which can effectively reduce the transition energy, greatly broaden the light absorption, and significantly narrow the band gap of Ti-oxo clusters.

To investigate the electronic structure of clusters Ti_8Fcdc_4 and $Ti_{10}Fcdc_2$, density functional theory (DFT) calculations were performed. Some of the highest-occupied molecular orbital (HOMO) and lowest-unoccupied molecular orbital (LUMO) are shown in Fig. 4. It can be seen that the HOMO, HOMO−1 and HOMO−2 orbitals of clusters Ti_8Fcdc_4 and $Ti_{10}Fcdc_2$ primarily lie on the Fe 3d orbitals and π orbitals of the cyclopentadienyl rings, as is known about the reported

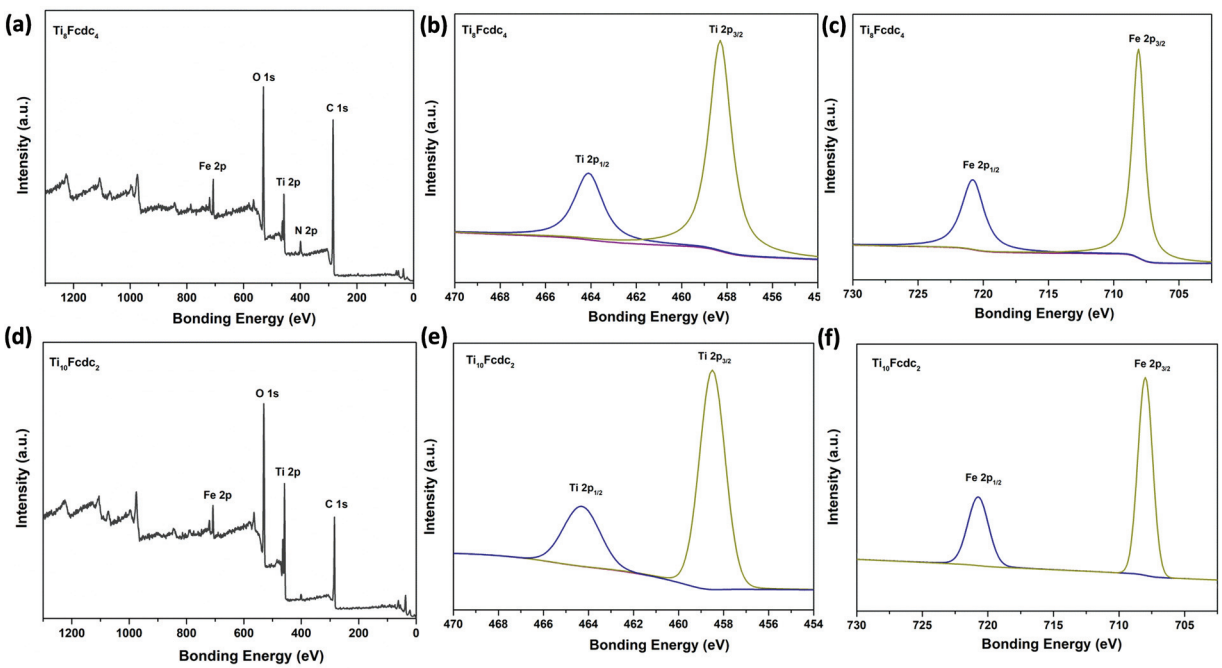

Fig. 2 The full-scan and high-resolution XPS spectrum of Ti_8Fcdc_4 (a–c) and $Ti_{10}Fcdc_2$ (d–f).

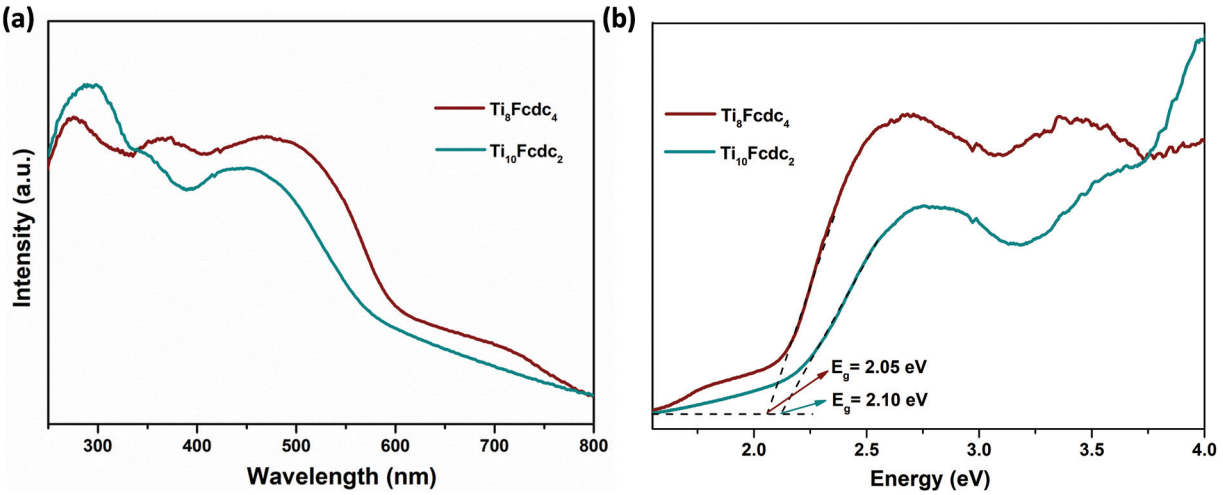

Fig. 3 (a) The solid-state UV–vis spectra of clusters Ti_8Fcdc_4 and $Ti_{10}Fcdc_2$. (b) Kubelka–Munk transformation of diffuse reflectance data of clusters Ti_8Fcdc_4 and $Ti_{10}Fcdc_2$.

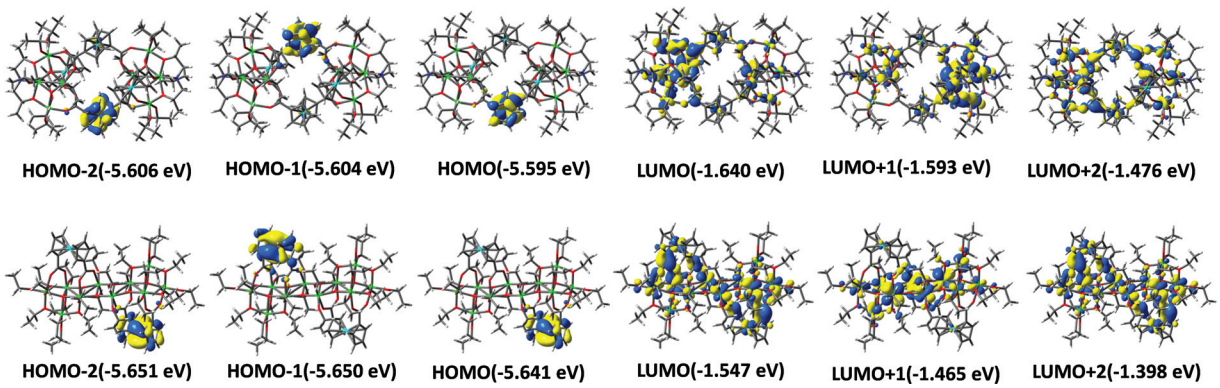

Fig. 4 Illustration of the coefficients of HOMOs and LUMOs of Ti_8Fcdc_4 (top) and $Ti_{10}Fcdc_2$ (bottom) based on DFT calculations.

ferrocene-sensitized Ti-oxo clusters.[55,60] The LUMO, LUMO+1 and LUMO+2 orbitals have a dominant contribution from the Ti 3d orbital of the TiO core. This suggests that the HOMO–LUMO charge transition is mainly related to the charge transfer from the Fcdc ligands to the Ti-oxo core.

The typical photoelectrochemical cell (PEC) was used to evaluate the photoelectrochemical activities of the ferrocene-sensitized Ti-oxo clusters. During the cyclic irradiation with Xe light (300 W), both Ti_8Fcdc_4 and $Ti_{10}Fcdc_2$-treated photoelectrodes display reversible transient short-circuit photocurrent responses (Fig. 5a), indicating the rapid photoinduced electron–hole separation in the photoelectrodes. It should be noted that the photocurrent intensity of the cluster Ti_8Fcdc_4-treated photoelectrode (0.50 μA cm^{-2}) is higher than that of the cluster $Ti_{10}Fcdc_2$-treated photoelectrode (0.38 μA cm^{-2}), which may be mainly ascribed to the different structures. As discussed above, in cluster Ti_8Fcdc_4, the Ti-oxo core is composed of two $Ti_4(\mu_3\text{-}O)_2$ subunits bridged by two Fcdc units, and each $Ti_4(\mu_3\text{-}O)_2$ subunit is further coordinated with additional Fcdc units. The bridged Fcdc ligands would provide potential transmission channels for electron transfer, thereby achieving its higher photoinduced charge transfer rate. In addition, two diisopropanolamine ligands as additional channels may also contribute to the efficient and fast electron transfer. However, when the photoelectrode is irradiated by a light source, the photocurrent intensity of clusters Ti_8Fcdc_4 and $Ti_{10}Fcdc_2$ does not reach the maximum immediately, which may be attributed to the reduced electron mobility, and this phenomenon has already appeared in the reported literature.[61] The IR spectra of the samples after the photocurrent measurements match well with the original spectra, indicating that these ferrocene-sensitized Ti-oxo clusters have good stability as the photoelectrode precursor materials (Fig. S9 and S10†).

The Mott–Schottky plots of ferrocene-sensitized Ti-oxo cluster–treated photoelectrodes are shown in Fig. 5b. The positive slope of the plots verifies that these two ferrocene-sensitized Ti-oxo clusters are n-type semiconductor materials. It is obvious that the slope of the Ti_8Fcdc_4-treated photoelectrode on the plot is lower than that of the $Ti_{10}Fcdc_2$-treated photo-

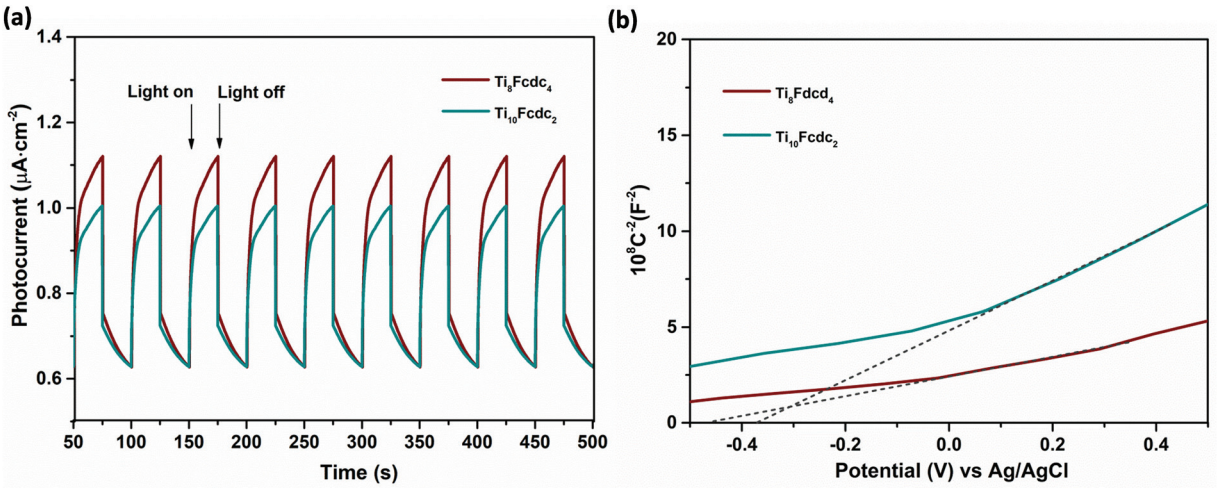

Fig. 5 (a) The photocurrent responses of clusters Ti_8Fcdc_4 and $Ti_{10}Fcdc_2$. (b) The Mott–Schottky plots of clusters Ti_8Fcdc_4 and $Ti_{10}Fcdc_2$.

electrode. As known, the slope of the linear region is inversely proportional to the donor density. This result of the Mott–Schottky plots showed that the carrier density of the **Ti_8Fcdc_4**-treated photoelectrode is higher than that of the **$Ti_{10}Fcdc_2$**-treated photoelectrode. As known, the carrier density is closely related to the electron injection efficiency. Thus, this result suggested that cluster **Ti_8Fcdc_4** has higher electron injection efficiency than cluster **$Ti_{10}Fcdc_2$**. The flat-band potential of **Ti_8Fcdc_4** and **$Ti_{10}Fcdc_2$**-treated photoelectrodes in terms of the plots is about −0.25 and −0.16 V (relative to NHE), respectively. For n-type semiconductors, the conduction band potential is lower than the flat-band potential (about 0.10 V). Hence the conduction band potentials of **Ti_8Fcdc_4** and **$Ti_{10}Fcdc_2$**-treated photoelectrodes are about −0.35 and −0.26 V (relative to NHE), respectively. Based on the band gap of clusters **Ti_8Fcdc_4** and **$Ti_{10}Fcdc_2$** (2.05 and 2.10 eV, respectively), the valence band potentials of **Ti_8Fcdc_4** and **$Ti_{10}Fcdc_2$**-treated photoelectrodes are 1.70 and 1.84 V (relative to NHE), respectively. Electrochemical impedance spectroscopy (EIS) was also investigated. It can be clearly seen from Fig. 6 that the electrochemical impedance of the **Ti_8Fcdc_4**-treated photoelectrode on the Nyquist plot is less than that of the **$Ti_{10}Fcdc_2$**-treated photoelectrode, indicating that the surface charge transfer rate of cluster **Ti_8Fcdc_4** is faster than that of cluster **$Ti_{10}Fcdc_2$**. Therefore, the charge separation efficiency of cluster **Ti_8Fcdc_4** is indeed higher than cluster **$Ti_{10}Fcdc_2$**, which is also in agreement with the photocurrent responses. It can be seen from above all that these Fcdc-sensitized Ti-oxo clusters have good application prospects in the field of photovoltaic cells owing to their excellent photoelectrochemical activity.

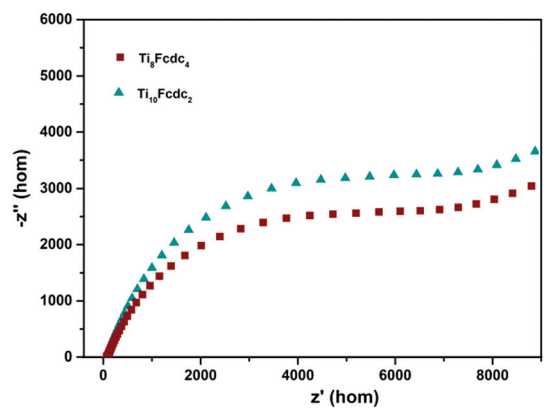

Fig. 6 Electrochemical impedance spectroscopy of clusters Ti_8Fcdc_4 and $Ti_{10}Fcdc_2$.

Conclusions

Two novel ferrocene-sensitized Ti-oxo clusters were synthesized and characterized. Thanks to the charge transfer from the ferrocene ligand to the Ti-oxo core, these two ferrocene-containing clusters exhibited intense visible light absorption. Moreover, the reversible photocurrent responses were also observed for cluster-treated photoelectrodes, indicating the rapid separation of photoinduced electrons and holes. Of note, cluster **Ti_8Fcdc_4** possesses substantially more enhanced photoelectrochemical activity than cluster **$Ti_{10}Fcdc_2$**, suggesting that the potential electron transport channel in cluster **Ti_8Fcdc_4** may be conducive to electron–hole separation. The ferrocene-sensitized cluster system provides valuable models for investigating the internal relationship between the structure and properties of sensitized clusters. Further studies on the synthetic chemistry, electronic structure and photoelectric properties of ferrocene-sensitized Ti-oxo cluster system are underway.

Author contributions

Chao Wang: conceptualization, methodology, resources, formal analysis, validation, writing-original draft, writing-

review and editing, funding acquisition. Shoujuan Wang: funding acquisition. Fangong Kong: funding acquisition. Ning Chen: validation.

Conflicts of interest

There are no conflicts to declare.

Acknowledgements

The project is supported by the Foundation (no. ZZ20200102) of State Key Laboratory of Biobased Material and Green Papermaking, Qilu University of Technology, Shandong Academy of Sciences.

Notes and references

1 N. Afzali, S. Tangestaninejad, R. Keshavarzi, V. Mirkhani, J. Nematollahi, M. Moghadam, I. Mohammadpoor-Baltork, M. Reimer, S. Olthof, A. Klein and S. H. Gimenez, Ti-based MOF with embedded RuO_2 nanoparticles: a highly efficient photoelectrode for visible light water oxidation, *ACS Sustainable Chem. Eng.*, 2020, **8**, 18366–18376.

2 Y. Yan, C. Q. Li, Y. H. Wu, J. K. Gao and Q. C. Zhang, From isolated Ti-oxo clusters to infinite Ti-oxo chains and sheets: recent advances in photoactive Ti-based MOFs, *J. Mater. Chem. A*, 2020, **8**, 15245–15270.

3 J. J. Zhu, P. Z. Li, W. H. Guo, Y. L. Zhao and R. Q. Zou, Titanium-based metal–organic frameworks for photocatalytic applications, *Coord. Chem. Rev.*, 2018, **359**, 80–101.

4 X. Chen and S. S. Mao, Titanium dioxide nanomaterials: synthesis, properties, modifications, and applications, *Chem. Rev.*, 2007, **107**, 2891–2959.

5 X. Wang, R. Xia, E. Muhire, S. Jiang, X. Hou and M. Gao, Highly enhanced photocatalytic performance of TiO_2 nanosheets through constructing TiO_2/TiO_2 quantum dots homojunction, *Appl. Surf. Sci.*, 2018, **459**, 9–15.

6 H. G. Yang, G. Liu, S. Z. Qiao, C. H. Sun, Y. G. Jin, S. C. Simth, J. Zou, H. M. Cheng and G. Q. Lu, Solvothermal synthesis and photoreactivity of anatase TiO_2 nanosheets with dominant {001} Facets, *J. Am. Chem. Soc.*, 2009, **131**, 4078–4083.

7 A. Fujishima, T. N. Rao and D. A. Tryk, Titanium dioxide photocatalysis, *J. Photochem. Photobiol., C*, 2000, **1**, 1–21.

8 X. Chen and S. S. Mao, Titanium dioxide nanomaterials: synthesis, properties, modifications, and applications, *Chem. Rev.*, 2007, **107**, 2891–2959.

9 J. Schneider, M. Matsuoka, M. Takeuchi, J. Zhang, Y. Horiuchi, M. Anpo and D. W. Bahnemann, Understanding TiO_2 photocatalysis: mechanisms and materials, *Chem. Rev.*, 2014, **114**, 9919–9986.

10 X. Chen, L. Liu, P. Y. Yu and S. S. Mao, Increasing solar absorption for photocatalysis with black hydrogenated titanium dioxide nanocrystals, *Science*, 2011, **331**, 746–750.

11 Y. Rao and W. Chu, Reaction mechanism of linuron degradation in TiO_2 suspension under visible light irradiation with the assistance of H_2O_2, *Environ. Sci. Technol.*, 2009, **43**, 6183–6189.

12 W. H. Fang, L. Zhang and J. Zhang, Synthetic strategies, diverse structures and tuneable properties of polyoxo-titanium clusters, *Chem. Soc. Rev.*, 2018, **47**, 404–421.

13 P. Coppens, Y. Chen and E. Trzop, Crystallography and properties of polyoxotitanate nanoclusters, *Chem. Rev.*, 2014, **114**, 9645–9661.

14 L. Rozes and C. Sanchez, Titanium-oxo-clusters: precursors for a Lego-like construction of nanostructured hybrid materials, *Chem. Soc. Rev.*, 2011, **40**, 1006–1030.

15 N. Li, P. D. Matthews, H. K. Luo and D. S. Wright, Novel properties and potential applications of functional ligand-modified polyoxotitanate cages, *Chem. Commun.*, 2016, **52**, 11180–11190.

16 P. D. Matthews, T. C. King and D. S. Wright, Structure, photochemistry and applications of metal doped polyoxotitanium alkoxide cages, *Chem. Commun.*, 2014, **50**, 12815–12823.

17 Y. J. Liu, W. H. Fang, L. Zhang and J. Zhang, Recent advances in heterometallic polyoxotitanium clusters, *Coord. Chem. Rev.*, 2020, **404**, 213099.

18 Q. Y. Zhu and J. Dai, Titanium-oxo/alkoxyl clusters anchored with photoactive ligands, *Coord. Chem. Rev.*, 2021, **430**, 213664.

19 W. H. Fang, L. Zhang and J. Zhang, A 3.6 nm Ti_{52}-oxo nanocluster with precise atomic structure, *J. Am. Chem. Soc.*, 2016, **138**, 7480–7483.

20 M. Y. Gao, F. Wang, Z. G. Gu, D. X. Zhang, L. Zhang and J. Zhang, Fullerene like polyoxotitanium cage with high solution stability, *J. Am. Chem. Soc.*, 2016, **138**, 2556–2559.

21 C. Zhao, Y. Z. Han, S. Dai, X. Chen, J. Yan, W. Zhang, H. Su, S. Lin, Z. Tang, B. K. Teo and N. F. Zheng, Microporous cyclic titanium-oxo clusters with labile surface ligands, *Angew. Chem., Int. Ed.*, 2017, **56**, 16252–16256.

22 Y. R. Zhao, H. Zheng, L. Q. Chen, H. J. Chen, X. J. Kong, L. S. Long and L. S. Zheng, The effect on the luminescent properties in lanthanide-titanium-oxo clusters, *Inorg. Chem.*, 2019, **58**, 10078–10083.

23 N. Li, D. Pranantyo, E. T. Kang, D. S. Wright and H. K. Luo, A simple drop-and-dry approach to grass-like multifunctional nano-coating on flexible cotton fabrics using in situ generated coating solution comprising titanium-oxo custers and silver nanoparticles, *ACS Appl. Mater. Interfaces*, 2020, **12**, 12093–12100.

24 N. Li, D. Pranantyo, E. T. Kang, D. S. Wright and H. K. Luo, In situ self-assembled polyoxotitanate cages on flexible cellulosic substrates: multifunctional coating for hydrophobic, antibacterial, and UV-blocking applications, *Adv. Funct. Mater.*, 2018, **28**, 1800345.

25 Y. P. He, G. H. Chen, D. J. Li, Q. H. Li, L. Zhang and J. Zhang, Combining titanium–organic cage and hydrogen-

bonded organic cage for highly effective third-order nonlinear optics, *Angew. Chem., Int. Ed.*, 2021, **60**, 2920–2923.
26 M. Czakler, C. Artner and U. Schubert, Two new hexanuclear titanium-oxo cluster types and their structural connection to known clusters, *New J. Chem.*, 2018, **42**, 12098–12103.
27 G. Zhang, C. Liu, D. L. Long, L. Cronin, C. H. Tung and Y. Wang, Water-soluble pentagonal–prismatic titanium-oxo clusters, *J. Am. Chem. Soc.*, 2016, **138**, 11097–11100.
28 Y. Z. Yu, Y. Guo, Y. R. Zhang, M. M. Liu, Y. R. Feng, C. H. Geng and X. M. Zhang, A series of silver doped butterfly-like Ti_8Ag_2 clusters with two Ag ions panelled on a Ti_8 surface, *Dalton Trans.*, 2019, **48**, 13423–13429.
29 X. Fan, J. H. Wang, K. F. Wu, L. Zhang and J. Zhang, Isomerism in titanium-oxo clusters: molecular anatase model with atomic structure and improved photocatalytic activity, *Angew. Chem., Int. Ed.*, 2019, **58**, 1320–1323.
30 H. Zheng, M. H. Du, S. C. Lin, Z. C. Tang, X. J. Kong, L. S. Long and L. S. Zheng, Assembly of a wheel like $Eu_{24}Ti_8$ cluster under the guidance of high resolution electrospray ionization mass spectrometry, *Angew. Chem., Int. Ed.*, 2018, **57**, 10976–10979.
31 K. Z. Su, M. Y. Wu, Y. X. Tan, W. J. Wang, D. Q. Yuan and M. C. Hong, A monomeric bowl-like pyrogallol[4]arene Ti_{12} coordination complex, *Chem. Commun.*, 2017, **53**, 9598–9601.
32 F. Pei, S. Q. Dai, B. F. Guo, H. Xie, C. W. Zhao, J. Q. Cui, X. L. Fang, C. M. Chen and N. F. Zheng, Titanium-oxo clusters reinforced gel polymer electrolyte enabling lithium-sulfur batteries with high gravimetric energy densities, *Energy Environ. Sci.*, 2021, **14**, 975–985.
33 Y. Chen, K. N. Jarzembska, E. Trzop, L. Zhang and P. Coppens, How does substitutional doping affect visible light absorption in a series of homodisperse Ti_{11} polyoxotitanate nanoparticles?, *Chem. – Eur. J.*, 2015, **21**, 11538–11544.
34 S. Eslava, M. McPartlin, R. I. Thomson, J. M. Rawson and D. S. Wright, Single-source materials for metal-doped titanium oxide: syntheses, structures, and properties of a series of heterometallic transition-metal titanium-oxo cages, *Inorg. Chem.*, 2010, **49**, 11532–11540.
35 X. Fan, F. R. Yuan, D. J. Li, S. Chen, Z. B. Cheng, Z. J. Zhang, S. C. Xiang, S. Q. Zang, J. Zhang and L. Zhang, Threefold collaborative stabilization of Ag_{14}-nanorods by hydrophobic Ti_{16}-Oxo clusters and alkynes: designable assembly and aolid-atate optical-limiting application, *Angew. Chem., Int. Ed.*, 2021, **60**, 12949–12954.
36 M. Y. Gao, Y. Y. Sun, F. Wang, J. Zhang and L. Zhang, Synthesis and structure of a series of Ti_6-oxo clusters functionalized by in situ esterified dicarboxylate ligands, *Chin. J. Chem.*, 2021, **39**, 1259–1264.
37 Y. Z. Yu, Y. R. Zhang, C. H. Geng, L. Sun, Y. Guo, Y. R. Feng, Y. X. Wang and X. M. Zhang, Precise and wide-ranged band-gap tuning of Ti_6-core-based titanium-oxo clusters by the type and number of chromophore ligands, *Inorg. Chem.*, 2019, **58**, 16785–16791.
38 H. Y. Wang, M. Y. Fu, H. L. Zhai, Q. Y. Zhu and J. Dai, Mono- and bismetalphenanthroline-substituted Ti_{12} clusters: structural variance and the effect on electronic state and photocurrent property, *Inorg. Chem.*, 2021, **60**, 12255–12262.
39 N. Li, S. Q. Zhao, X. R. Ding, X. Y. Hu, Q. K. Zhang, G. D. Zou and Y. Fan, 8-hydroxyquinoline functionalized titanium-oxo clusters for visible-light-driven photocatalytic oxidative desulfurization, *Inorg. Chem. Commun.*, 2021, **130**, 108681.
40 J. B. Benedict and P. Coppens, The crystalline nanocluster phase as a medium for structural and spectroscopic studies of light absorption of photosensitizer dyes on semiconductor surfaces, *J. Am. Chem. Soc.*, 2010, **132**, 2938–2944.
41 R. C. Snoeberger, K. J. Young, J. Tang, L. J. Allen, R. H. Crabtree, G. W. Brudvig, P. Coppens, V. S. Batista and J. B. Benedict, Interfacial electron transfer into functionalized crystalline polyoxotitanate nanoclusters, *J. Am. Chem. Soc.*, 2012, **134**, 8911–8917.
42 J. D. Sokolow, E. Trzop, Y. Chen, J. Tang, L. J. Allen, R. H. Crabtree, J. B. Benedict and P. Coppens, Binding modes of carboxylate- and acetylacetonate-linked chromophores to homodisperse polyoxotitanate nanoclusters, *J. Am. Chem. Soc.*, 2012, **134**, 11695–11700.
43 J. L. Hou, Y. G. Weng, P. Y. Liu, L. N. Cui, Q. Y. Zhu and J. Dai, Effects of the ligand structures on the photoelectric activities, a model study based on titanium-oxo clusters anchored with S-heterocyclic ligands, *Inorg. Chem.*, 2019, **58**, 2736–2743.
44 G. H. Chen, Y. P. He, F. P. Liang, L. Zhang and J. Zhang, A green separation process of Ag via a $Ti_4(embonate)_6$ cage, *Dalton Trans.*, 2021, **49**, 17194–17199.
45 D. H. Zou, L. N. Cui, P. Y. Liu, S. Yang, Q. Y. Zhu and J. Dai, Molecular model of dye sensitized titanium oxides based on aryl-amine dye anchored titanium-oxo clusters, *Inorg. Chem.*, 2019, **58**, 9246–9252.
46 C. F. A. Negre, K. J. Young, M. B. Oviedo, L. J. Allen, C. G. Sánchez, K. N. Jarzembska, J. B. Benedict, R. H. Crabtree, P. Coppens, G. W. Brudvig and V. S. Batista, Photoelectrochemical hole injection revealed in polyoxotitanate nanocrystals functionalized with organic adsorbates, *J. Am. Chem. Soc.*, 2014, **136**, 16420–16429.
47 L. N. Cui, P. Y. Liu, L. Yang, X. P. Shu, Q. Y. Zhu and J. Dai, A series of Ti_6-oxo clusters anchored with arylamine dyes: effect of dye structures on photocurrent responses, *Chem. – Asian J.*, 2019, **14**, 3198–3204.
48 J. X. Liu, M. Y. Gao, W. H. Fang, L. Zhang and J. Zhang, Bandgap engineering of titanium-oxo clusters: labile surface sites used for ligand substitution and metal incorporation, *Angew. Chem., Int. Ed.*, 2016, **55**, 5160–5165.
49 W. L. Wu, G. Y. Zhang, J. Zhang, G. Wang, C. H. Tung and Y. F. Wang, Aerobic oxidation of toluene and benzyl alcohol to benzaldehyde using a visible light-responsive titanium-oxide cluster, *Chem. Eng. J.*, 2021, **404**, 126433.

50 B. C. Zhu, Q. L. Hong, X. F. Yi, J. Zhang and L. Zhang, Supramolecular co-assembly of the Ti_8L_{12} cube with [Ti $(DMF)_6$] species and Ti_{12}-oxo cluster, *Inorg. Chem.*, 2020, **59**, 8291–8297.

51 J. L. Hou, P. Huo, Z. Z. Tang, L. N. Cui, Q. Y. Zhu and J. Dai, A titanium-oxo cluster model study of synergistic effect of cocoordinated dye ligands on photocurrent responses, *Inorg. Chem.*, 2018, **57**, 7420–7427.

52 F. Jäkle and J. B. Sheridan, Ferrocenes: ligands, materials and biomolecules, *Angew. Chem., Int. Ed.*, 2008, **47**, 7587–7587.

53 S. K. Singh, R. Chauhan, B. Singh, K. Diwan, G. Kociok-Köhn, L. Bahadur and N. Singh, Enhanced light harvesting efficiencies of bis(ferrocenylmethyl)-based sulfur rich sensitizers used in dye sensitized TiO_2 solar cells, *Dalton Trans.*, 2012, **41**, 1373–1380.

54 Z. C. Liu, J. Y. Lei, M. Frasconi, X. H. Li, D. Cao, Z. X. Zhu, S. T. Schneebeli, G. C. Schatz and J. F. Stoddart, A square-planar tetracoordinate oxygen-containing Ti_4O_{17} cluster stabilized by two 1,1′-Ferrocenedicarboxylato ligands, *Angew. Chem., Int. Ed.*, 2014, **53**, 9193–9197.

55 Y. Fan, H. M. Li, R. H. Duan, H. T. Lu, J. T. Cao, G. D. Zou and Q. S. Jing, Phosphonate-stabilized titanium-oxo clusters with ferrocene photosensitizer: structures, photophysical and photoelectrochemical properties, and DFT/TDDFT calculations, *Inorg. Chem.*, 2017, **56**, 12775–12782.

56 Y. Fan, Y. Cui, G. D. Zou, R. H. Duan, X. Zhang, Y. X. Dong, H. T. Lv, J. T. Cao and Q. S. Jing, Ferrocenecarboxylate-functionalized titanium-oxo-cluster: ferrocene wheel as sensitizer for photocurrent response, *Dalton Trans.*, 2017, **46**, 8057–8064.

57 Y. Fan, Y. Zhang, G. D. Zou, H. M. Li, Y. Cui, Q. S. Jing and H. T. Lu, Modulating the band gap and photoelectrochemical activity of dicarboxylate-stabilized titanium-oxo clusters, *Inorg. Chim. Acta*, 2018, **482**, 16–22.

58 H. T. Lv, Y. Cui, Y. M. Zhang, H. M. Li, G. D. Zou, R. H. Duan, J. T. Cao, Q. S. Jing and Y. Fan, A 4-dimethylaminobenzoate-functionalized Ti_6-oxo cluster with a narrow band gap and enhanced photoelectrochemical activity: a combined experimental and computational study, *Dalton Trans.*, 2017, **46**, 12313–12319.

59 Y. Cui, P. F. Liu, M. Li, X. Zhang, T. M. Tang, G. D. Zou and Y. Fan, Structures, photoelectrochemical and photocatalytic properties of phosphite-stabilized titanium-oxo clusters functionalized with ferrocenecarboxylate ligands, *J. Cluster Sci.*, 2019, **30**, 1519–1524.

60 J. J. Liu, N. Li, J. W. Sun, J. Liu, L. Z. Dong, S. J. Yao, L. Zhang, Z. F. Xin, J. W. Shi, J. X. Wang, S. L. Li and Y. Q. Lan, Ferrocene-functionalized polyoxo-titanium cluster for CO_2 photoreduction, *ACS Catal.*, 2021, **11**, 4510–4519.

61 E. M. Han, W. D. Yu, L. J. Li, X. Y. Yi, J. Yan and C. Liu, Accurate assembly of ferrocene-functionalized $\{Ti_{22}Fc_4\}$ clusters with photocatalytic amine oxidation activity, *Chem. Commun.*, 2021, **57**, 2792–2795.

62 C. Wang, C. Liu, L. J. Li and Z. M. Sun, Synthesis, crystal structures, and photochemical properties of a family of heterometallic titanium-oxo clusters, *Inorg. Chem.*, 2019, **58**, 6312–6319.

63 C. Wang, C. Liu, X. He and Z. M. Sun, A cluster-based mesoporous Ti-MOF with sodalite supercages, *Chem. Commun.*, 2017, **53**, 11670–11673.

64 C. Wang, C. Liu, H. R. Tian, L. J. Li and Z. M. Sun, Designed cluster assembly of multidimensional titanium coordination polymers: syntheses, crystal structure and properties, *Chem. – Eur. J.*, 2018, **24**, 2952–2962.

65 C. Wang, S. J. Wang and F. G. Kong, Calixarene-protected titanium-oxo clusters and their photocurrent responses and photocatalytic performances, *Inorg. Chem.*, 2021, **60**, 5034–5041.

66 C. Wang, Y. J. Lu, M. Y. Rao, N. Chen, S. J. Wang and F. G. Kong, Co-crystal of Ti_4Ni_2 and Ti_8Ni_4 clusters with enhanced photochemical properties, *CrystEngComm*, 2021, **23**, 4402–4407.

67 C. Wang, J. S. Zhang and X. X. Zhu, Synthesis of lanthanide-doped titanium-oxo clusters for efficient photocurrent responses, *J. Solid State Chem.*, 2021, **304**, 122586.

68 G. M. Sheldrick, Crystal structure refinement with SHELXL, *Acta Crystallogr., Sect. C: Struct. Chem.*, 2015, **71**, 3–8.

69 O. V. Dolomanov, L. J. Bourhis, R. J. Gildea, J. A. K. Howard and H. Puschmann, OLEX2: a complete structure solution, refinement and analysis program, *J. Appl. Crystallogr.*, 2009, **42**, 339–341.